JMEPEG (2022) 31:6533–6544
https://doi.org/10.1007/s11665-022-06723-6

1059-9495/$19.00

TECHNICAL ARTICLE

Effect of Hot Extrusion Ratio on the Mechanical Properties and Microstructure of a 0.5 wt.% Graphene Nanoplatelet-Reinforced Aluminum Matrix Composite

Shumei Lou, Lingwei Ran, Yongqiang Liu, Peng Chen, Chunjian Su, and Qingbiao Wang

Submitted: 2 October 2021 / Revised: 16 December 2021 / Accepted: 17 January 2022 / Published online: 28 February 2022

A 0.5 wt.% graphene nanoplatelet-reinforced aluminum composite (0.5 wt.% GNPs/Al composite) was prepared by powder metallurgy and extruded at ratios of 8:1, 11:1, 17:1, 25:1 and 36:1 to study the effects of the extrusion ratio on the mechanical properties and microstructure of the composite. It is found that the composite shows the best general mechanical properties at an extrusion ratio of 17:1 tensile strength of 164.49 MPa, elongation of 21.81%, bending strength of 325.47 MPa, and a Young's modulus of 62.01 GPa. An extrusion ratio (8:1 or 11:1) that is too low results in poor grain refinement, separation of the GNP layers and ordinary properties. However, an extrusion ratio that is too large can also lead to grain growth (such as 25:1) or a reduction in GNP integrity (such as 36:1), which affects the strengthening efficiency of hot extrusion negatively.

Keywords 0.5 wt.% GNP/Al composite, extrusion ratio, hot extrusion, mechanical properties, microstructure

1. Introduction

With the rapid development of aerospace, machinery, and rail transportation, traditional metals can no longer fit into some special environments. As a new type of material, graphene-reinforced metal matrix composites combine the ductility and toughness of metals with the high strength and high elastic modulus of graphene (Ref 1, 2), resulting in high strength, plasticity and elastic modulus. Aluminum and aluminum alloys have the advantages of good plasticity, high toughness, high specific strength, low density, good conductivity and low price (Ref 3-7) and are widely used as the matrix in composites. Therefore, graphene or graphene nanoplatelet (GNP)-reinforced aluminum composites have attracted the attention of researchers (Ref 8-11). During the preparation of composites, the hot extrusion process (Ref 12-16), as a secondary process, can lead to the deformation of graphene-reinforced metal composites under the dual action of temperature and pressure (Ref 8, 17-20), improving the compactness of the material, better dispersion of the GNP (Ref 8) and refining the grains (Ref 8, 21), thus improving the mechanical properties of the composite.

Many scholars have studied the effect of extrusion on the properties of metal matrix composites. Xu et al. (Ref 22) prepared CNT/Al composites by powder metallurgy and hot extrusion at 500 °C with an extrusion ratio of 36:1. The tensile strength of the composite after hot extrusion is 312 MPa, and the elongation is 15.8%. Wang et al. (Ref 23) conducted a hot extrusion test on the prepared TC4p/AZ91 composite. After extrusion, the tensile strength of the material reached 369 MPa, and the elongation rate was 6.4%, which was greatly improved after extrusion. During the extrusion process, TC4 can refine the grains and undergo plastic deformation so that the composite exhibits excellent comprehensive mechanical properties. Yang et al. (Ref 24) prepared TiB2/Al composites by powder metallurgy and hot extrusion. The grains obtained by hot extrusion are more refined than those obtained by hot pressing, indicating that dynamic recrystallization (Ref 25, 26) occurs during the extrusion process. Allah Ditta (Ref 27) et al. prepared a Zn-rich Al-11.3Zn-2.65Mg-1Cu alloy by spray forming rapid solidification technology, which showed a yield strength as high as 807 MPa after hot extrusion and tempering. Lei et al. (Ref 28) studied the microstructure, mechanical properties and corrosion properties of Mg-11Li-3Al-2Zn-1.5Nd-0.2Zr alloy before and after hot extrusion. The tensile strength and elongation of the extruded alloy were 149.86 MPa and 42.33%, respectively, which is higher than that of the homogeneous alloy. It is concluded that the improvement of mechanical properties and corrosion resistance of the alloy after hot extrusion is the result of grain refinement and uniform distribution of the intermetallic phases.

Extrusion process parameters have an important influence on the microstructure and mechanical properties of materials, so many scholars have conducted certain studies on the parameters of the hot extrusion process. Shao et al. (Ref 29) studied the mechanical properties of 0.6 wt.% GNP/6061Al composites at different temperatures. For a compression temperature of 450 °C, the yield strength and tensile strength of the composite reach the highest values, which are increased by 16 and 40.1%, respectively, compared with the unreinforced matrix. Yu et al. (Ref 30) studied the microstructure and mechanical properties

Shumei Lou, Lingwei Ran, Yongqiang Liu, Peng Chen, and **Chunjian Su**, Department of Mechanical and Electrical Engineering, Shandong University of Science and Technology, Qingdao 266590 Shandong, China; **Qingbiao Wang**, Composite Industry Research Institute, Shandong University of Science and Technology, Taian 271019 Shandong, China. Contact e-mail: skd992951@sdust.edu.cn.

of Mg-Y(nd/Zn)-Zr alloys at different extrusion temperatures. It was found that with increasing extrusion temperature, the strength of the alloy decreases and the plasticity increases. El sayed seleman (Ref 31) et al. prepared 5, 10, 15 and 20 wt.% GNPs/6016Al alloys and hot extruded them at 450 °C. After extrusion, the hardness value of the GNP/6016Al composite was higher than that of the matrix, and the wear resistance of the GNP/6016Al composite increased as the graphene content increased. The wear resistance of the 20 wt.% GNP/6016Al composite was found to be 10 times higher than that of the pure alloy.

In summary, several researchers have mainly studied the influence of extrusion temperature, GNP percentage or extrusion speed on the microstructure and mechanical properties of graphene-reinforced metal composites, but few studies have been reported about the influence of the extrusion ratio.

In the hot extrusion process, the extrusion ratio is a very important parameter that largely affects the distribution of stress, the degree of work hardening, grain refinement, dynamic recrystallization and dynamic recovery. Therefore, it is necessary to study the influence of the extrusion ratio on GNP-reinforced metal matrix composites. In this paper, a 0.5 wt.% GNP-reinforced aluminum matrix composite (0.5 wt.% GNPs/Al composite) was hot extruded with different extrusion ratios. The influence of the extrusion ratio on the microstructure and mechanical properties of the composite was explored, providing a reference for the optimization of the process parameters and industrialization of the hot extrusion process for GNP/Al composites.

2. Experimental

2.1 Preparation of the Composite

The matrix of the composite was composed of spherical Al powder purchased from Henan Ocean Powder Technology Co., Ltd. The purity was over 99.98%, and the particle size was 18 μm. Figure 1(a) shows a scanning electron microscopy (SEM) image of the pure aluminum powder. GNPs were purchased from Qingdao Huagao Graphene Technology Co., Ltd., with approximately 10-20 layers, a specific surface area of approximately 230 m^2/g and a diameter ranging from approximately 2 μm to 4 μm. Figure 1(b) shows a transmission electron microscope (TEM) image of the GNPs, with typical flocculent and translucent wrinkled structure characteristics.

GNPs were mixed in absolute ethanol with a mass fraction of 0.5% and sonicated for 90 min. Subsequently, aluminum powder was added to the graphene solution. Then, the 0.5 wt.% GNPs/Al mixed composite was ball milled using a planetary ball mill at a speed of 300 r/min for 6 h, which is the optimized parameter we obtained in our previous work (Ref 32). Then, the milled powder was dried in a vacuum drying oven and solidified in a vacuum hot-pressed sintering furnace. The sintering temperature was 570 °C, the sintering pressure was 30 MPa, and the holding time was 90 min. Following this, the sample was cooled in the furnace for 2 h, obtaining a 0.5 wt.% cylindrical GNP/Al composite billet with a size of φ 42 × 30 mm.

2.2 Hot Extrusion

The cylindrical GNP/Al composite billet was hot extruded using a 200-ton computer-controlled servo-hydraulic press at an extrusion rate of 1 mm/min. The extrusion temperature was 490 °C, and the extrusion die angle was 90° with extrusion ratios of 8:1, 11:1, 17:1, 25:1 and 36:1. For the convenience of description, the five groups of test subjects are named as follows: R-8@GNPs/Al, R-11@GNPs/Al, R-17@GNPs/Al, R-25@GNPs/Al, and R-36@GNPs/Al, as indicated in Table 1. Before hot extrusion, the surfaces of the blank were mechanically polished to remove the oxide scale. The extruded profile was quenched to retain the microstructure of the extruded profile.

2.3 Microstructural Characterization

All the samples were taken from the central shaft section of the extruded bar. A Raman spectrometer (Horiba LabRAM HR evolution), field emission SEM (FESEM, Sigma-300) and electron backscattering diffraction (EBSD) were used to observe the microstructure of the GNP/Al composite. The laser wavelength of the Raman spectrometer was 532 nm. SEM was used to observe the tensile fracture morphology of the samples and the morphology of the GNPs. Then, the EBSD samples were prepared by electrolytic polishing to analyze the grain orientation and grain boundary distribution of the composite.

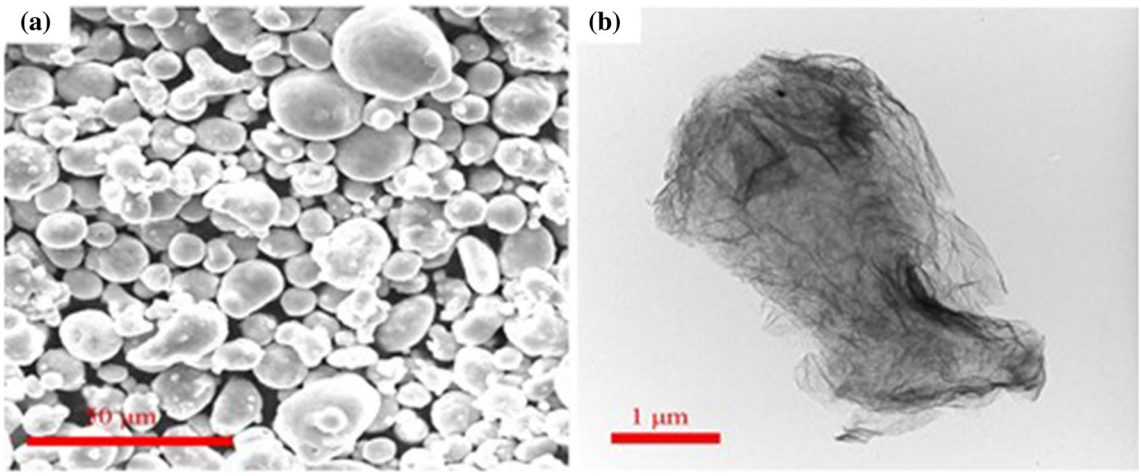

Fig. 1 (a) SEM image of pure aluminum powder; (b) TEM images of graphene

Table 1 Extrusion parameters

Groups	Extrusion temperature *T*, °C	Extrusion ratio	Extrusion die Angle, °
R-8@GNPs/Al	490	8:1	90
R-11@GNPs/Al	490	11:1	90
R-17@GNPs/Al	490	17:1	90
R-25@GNPs/Al	490	25:1	90
R-36@GNPs/Al	490	36:1	90

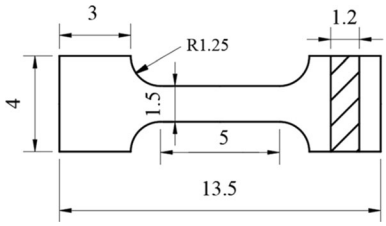

Fig. 2 The tensile sample (unit mm)

The dimensions of the EBSD specimen were 8 × 8 × 1 mm. All the observation surfaces of the SEM and EBSD are parallel to the extrusion direction.

2.4 Mechanical Performance

An electronic universal tensile testing machine (Zwick Z2.5 TH) was used for room temperature tensile testing, and a laser extensometer was used to measure the elongation and elastic modulus. The dimensions of the tensile specimen based on ISO 6892-1:2009, MOD are shown in Fig. 2. The gauge length was 5 mm, and the stretching rate was 1 mm/min. An electronic material testing machine (INSTRON E1000) was used to perform three-point bending tests (ISO 7438: 2005, MOD), as shown in Fig. 3. Both the lengths of the tensile and bending samples are taken along the extrusion direction. To ensure that the measurement results were scientific and effective, three samples were taken in each case for the tensile and bending tests. A microhardness tester (THVS-MA) was used to test the microhardness of the composites with different hot extrusion ratios. The test load was 25 g, and the loading time was 10 s. Ten different positions were tested for each sample. The maximum and minimum values were removed, and then, the average value was taken as the microhardness of the sample to ensure the accuracy of the data.

3. Results and Discussion

3.1 Effect of Extrusion Ratio on the Microstructures of the Composite

Raman spectroscopy characterization and EBSD testing were carried out to study the effect of the extrusion ratio on the microstructure of the extruded composite.

3.1.1 Raman Spectroscopy Characterization. Figure 4 shows the Raman spectra for the composite extruded with different extrusion ratios. From our previous work (Ref 8, 32), it could be concluded that after hot extrusions, the agglomeration and the layer number of the GNP will be decreased and the dispersion of GNP will be increased. So the values of I_D/I_G will decrease and the values of I_{2D}/I_G ratio will increase. Furthermore, with increasing of the extrusion ratios, the I_D/I_G ratios first decrease and then increase. This is because with increasing extrusion ratio, GNPs are subjected to greater shear stress due to more serious flow of the aluminum matrix, which can give rise to more layer separations and new graphene surfaces, reducing the I_D/I_G ratio value, which is the smallest with an extrusion ratio of 25:1. Moreover, the variation trend of the I_{2D}/I_G ratio also proves that the layer separation of GNPs becomes more obvious and that more new surfaces are generated with the increasing of the extrusion ratio. For R-36@GNPs/Al composite, the I_{2D}/I_G ratio is the lowest so the layer number should be the least. But at the same time, the I_D/I_G ratio of the R-36@GNPs/Al composite is the highest. This is because if the extrusion ratio is too large, the shear stress on the GNPs becomes too large, which will lead to fragmentation and a reduction in the diameter of the GNPs and forming a lot of defects in the GNPs.

3.1.2 Grain Orientations. Figure 5 shows EBSD images of the longitudinal sections along the extrusion direction (ED) of the composite extruded with extrusion ratios of 11:1, 17:1 and 25:1. Figure 6 shows the misorientation angles of the composite extruded with extrusion ratios of 11:1, 17:1 and 25:1. Figure 5(a) shows that the grain orientation characteristic along the extrusion direction of R-11@GNPs/Al composite is very obvious. Almost no dynamic recrystallization occurs, and the average grain size is 7.14 μm. It can also be observed from Fig. 6(a) that there are a small number of low-angle boundaries in the large oriented grains. The proportion of high misorientation angles in R-11@GNPs/Al is 51.37%. This is because a smaller extrusion ratio for the composite leads to a smaller triaxial compressive stress during hot extrusion (Ref 33), and fewer dislocations result in less dynamic recovery and corresponding subgrain generation. Figure 5(c) shows EBSD images of R-17@GNPs/Al, in which some fibrous crystal grains transform into fine crystal grains because the larger extrusion ratio leads to more energy and higher temperature to promote partial continuous dynamic recrystallization, and the average grain size becomes 4.98 μm. At the same time, the work hardening effect is improved, the deformation dislocations and the subgrain boundaries generated by dynamic recovery coexist, so the proportion of high misorientation angles is reduced to 48.24%, as shown in Fig. 6(b). When the extrusion ratio continues to increase to 25:1, as shown in Fig. 5(e), most of the grains are oriented to some extent, and the average grain size increases to 8.6 μm. This is because the extrusion ratio is large, more energy is generated during the extrusion process, which leads to an increase in the local temperature of the composite, promoting dynamic recovery as well as the

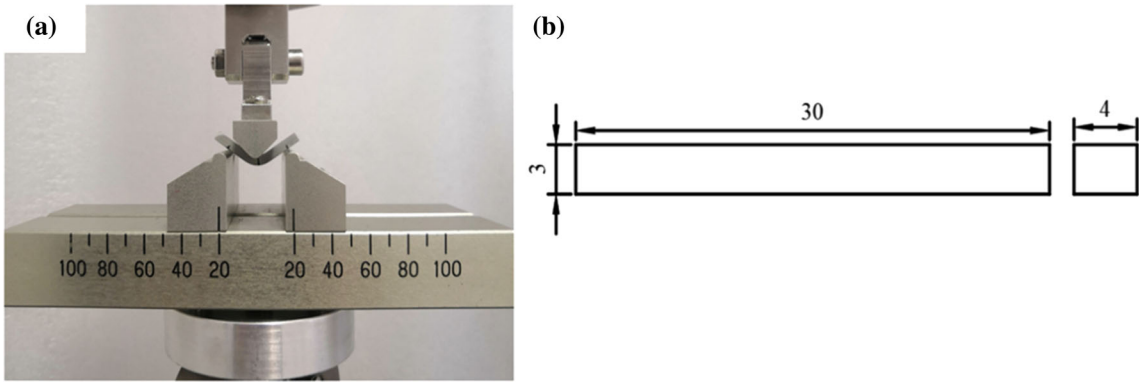

Fig. 3 Three-point bending at room temperature. (a) Three-point bending test; (b) dimension of the specimen (unit: mm)

according to generation of subgrains with low misorientation angles and recrystallization; however, at the same time, the recrystallized grains grow. Therefore, the proportion of the high misorientation angle decreases to 40.34%, as shown in Fig. 6(c).

The strength of the composite is closely related to its grain size. Grain refinement is the main method to improve the strength of composites (Ref 34-36). The contribution of refined grains to improving the yield strength of composites can be expressed by the Hall–Petch (Ref 13, 37) formula as follows:

$$\Delta\sigma_{CD} = K\left(D_A^{-0.5} - D_B^{-0.5}\right)$$

where $\Delta\sigma_{CD}$ is the change in yield strength of the composite due to grain refinement. K: Material-related parameter, 0.04 MPa $m^{1/2}$ for the composite in this paper. D_B, D_A: The average grain size before and after hot extrusion.

Among the composites extruded with different extrusion ratios, the average grain size of the R-17@GNPs/Al composite is 4.98 μm, which is much smaller than that obtained for other extrusion parameters. According to the Hall–Petch formula, the refined grains make a greater contribution to the strength improvement of the composite.

Figure 7 shows the inverse pole diagram for (100) (the plane perpendicular to ED) of the composite extruded with extrusion ratios of 11:1, 17:1 and 25:1. For an extrusion ratio of 11:1, textures $<111>$ and $<001>$ coexist, but the main orientation is $<111>$. However, as the extrusion ratio increases, the strength of the $<111>$ texture gradually increases. Meanwhile, when the extrusion ratio is 11:1 and 25:1, the $<001>$ texture orientation also appears, as shown in Fig. 7(a) and (c). An extrusion ratio that is too large or too small is conducive to the arbitrary growth and coarsening of the broken fine grains (Ref 30), resulting in evolution of the grain orientation and weakening of the consistency of the texture orientation.

3.2 Effect of Extrusion Ratio on Mechanical Properties of the Composite

3.2.1 Tensile Properties. The stress–strain curve obtained from the tensile test is shown in Fig. 8, and the detailed tensile strength and elongation of the composite are shown in Fig. 9. It can be seen that the tensile strength of the hot-pressed composite is 71.77MPa, and the elongation is 0.76% due to the relative low hot pressing temperature aimed at avoiding too much activity of the GNP and the aluminum (Ref 8). The R-8@GNPs/Al composite shows a tensile strength of 131.6 MPa and an elongation of 18.95%. As the extrusion ratio increases, the tensile strength of the composite first increases and then decreases. The R-17@GNPs/Al composite shows the best tensile performance, with a tensile strength of 164.49 MPa and an elongation of 21.81%, which represent an increase of 24.99 and 15.09%, respectively, compared with the R-8@GNPs/Al composite. As the extrusion ratio continues to increase, the mechanical properties of the composite show a decline trend. The tensile strength of the R-25@GNPs/Al composite is 150.01 MPa, and the elongation rate is 18.82%. When the extrusion ratio is small (8:1 or even 11:1), the effects of hot extrusion on the compaction of the composite and on the dispersion, orientation arrangement and delamination of the GNPs are limited because of the relatively small normal and shear stresses. The agglomeration of the GNPs contributes to the crack initiation. When the extrusion ratio is too large (25:1 or even 36:1), the dislocation density further increases, and the larger extrusion ratio leads to the flow stress and temperature of the material to increase, resulting in an increase in the grain size (Figs. 5e, f) and the accordingly the decline of the tensile properties.

3.2.2 Bending Properties. Figure 10 shows the three-point bending load–displacement curves for the composite hot-pressed or extruded with different extrusion ratios. It can be seen from Fig. 10 that the maximum load that the hot-pressed composite can bear is only 165.1 N and the vertical displacement of the indenter is 0.3 mm. The crack shows a brittle style. After hot extrusions, the maximum load the composite can bear is improved greatly. When the extrusion ratio is 8, the maximum load and displacement of the bending indenter for the composite with extrusion ratios of 8 and 11 are 307.66 N, 320.38 N and 7.51, 7.42 mm, respectively. When the extrusion ratio is 17, the composite material exhibits the best bending resistance, with a maximum load of 380.99 N (The calculate bending strength is 325.47 MPa) and the vertical displacement of 5.72 mm indicating the best bending strength and stiffness;

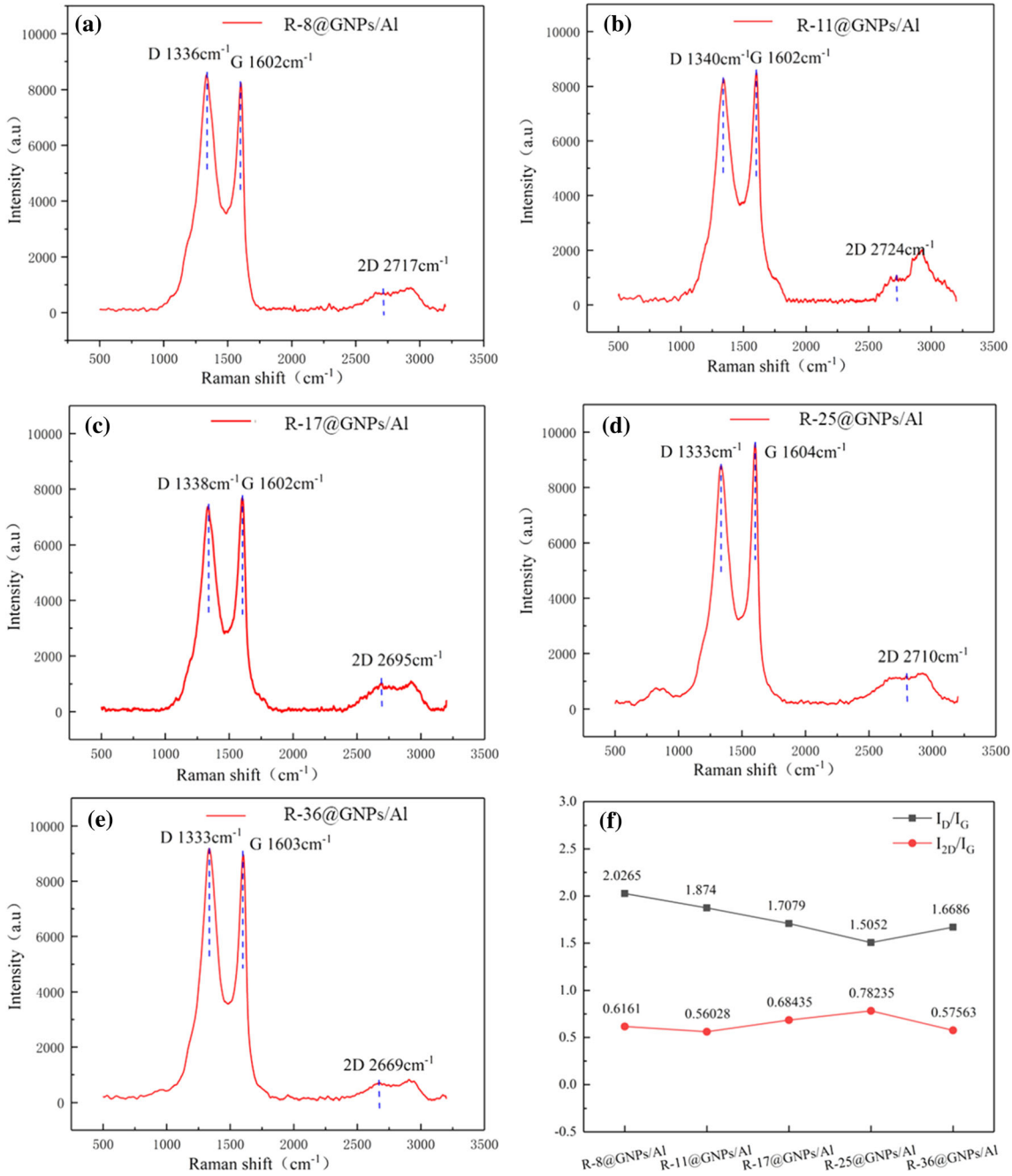

Fig. 4 Raman spectra of the composite extruded with different extrusion ratios: (a)R-8@GNPs/Al; (b) R-11@GNPs/Al; (c) R-17@GNPs/Al; (d) R-25@GNPs/Al; (e) R-36@GNPs/Al; (f) I_D/I_G and I_{2D}/I_G ratios

when the extrusion ratio is 25, the maximum load of the composite material is 337.56 N, and the vertical displacement is 7 mm, when the extrusion ratio is 36, the maximum load of the composite is 322.05 N, and the vertical displacement is 7.6 mm.

3.2.3 Young's Modulus and Vickers Hardness. Figure 11 shows the Young's modulus of the composite with different extrusion ratios. The Young's modulus also generally shows the same trend as the tensile and bending strengths. The Young's modulus of the R-17@GNPs/Al composite is the largest, with a value of 62.01 GPa. The R-25@GNPs/Al composite shows a Young's modulus of 52.98 GPa.

Figure 12 shows the Vickers hardness of the composite hot-pressed or extruded with different extrusion ratios. The hardness of the hot-pressed composite is 31.08HV. It can be observed that the R-11@GNPs/Al composite shows a hardness

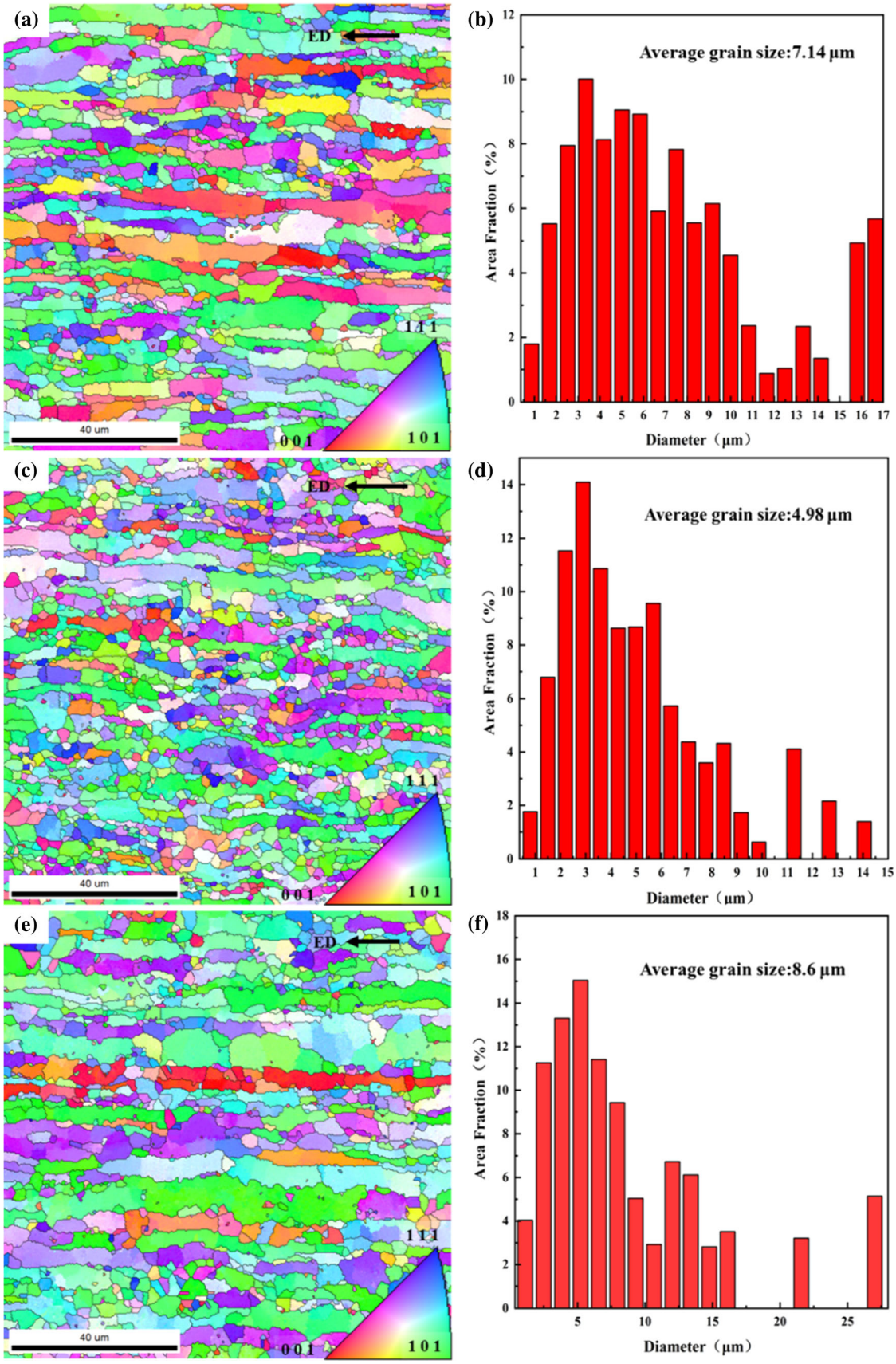

Fig. 5 EBSD and grain size distribution of the composite with different extrusion ratios: (a, b) R-11@GNPs/Al; (c, d) R-17@GNPs/Al; (e, f) R-25@GNPs/Al

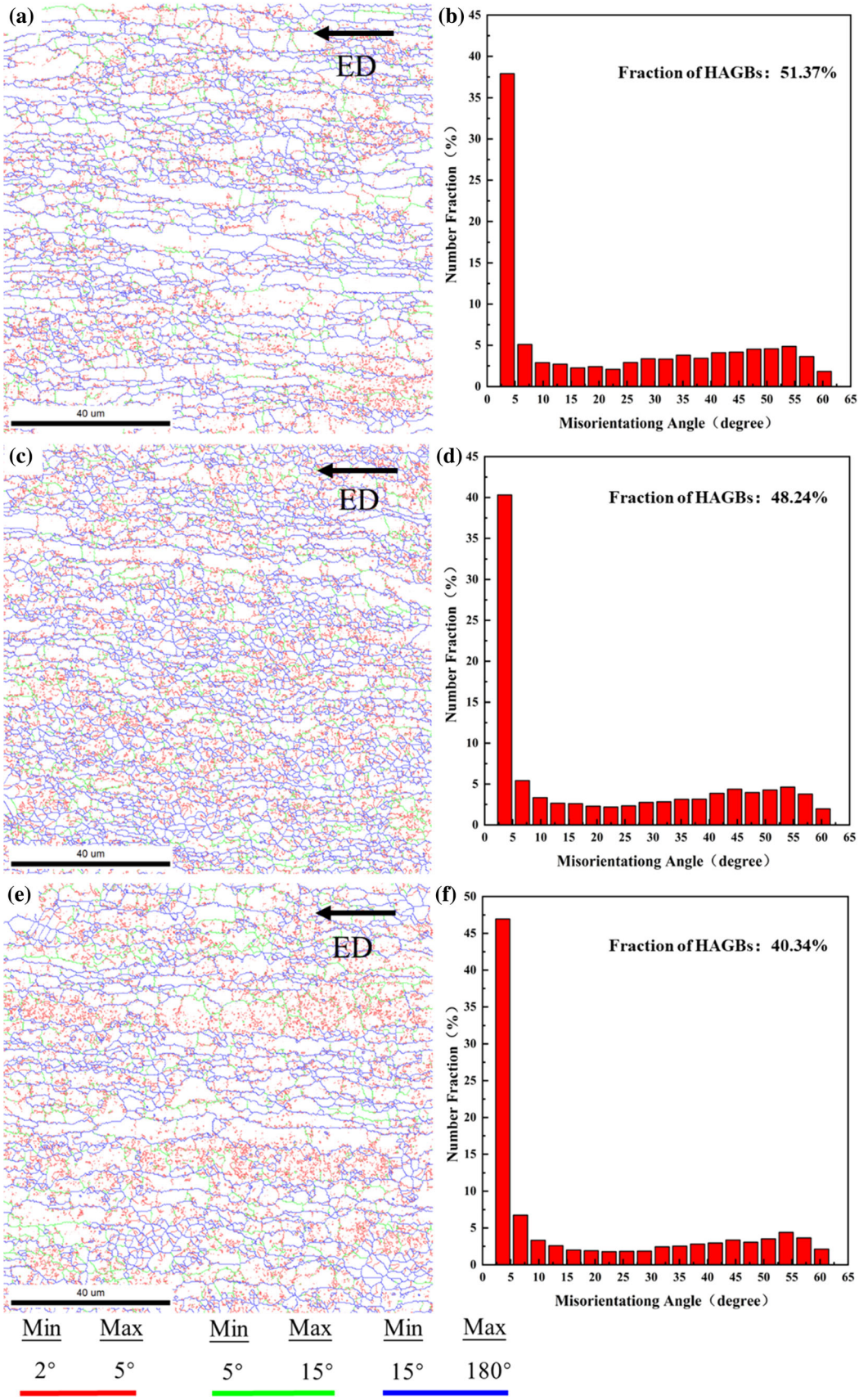

Fig. 6 Misorientation angle and its distribution of the composite extruded with different extrusion ratios: (a, b) R-11@GNPs/Al; (c, d) R-17@GNPs/Al; (e, f) R-25@GNPs/Al

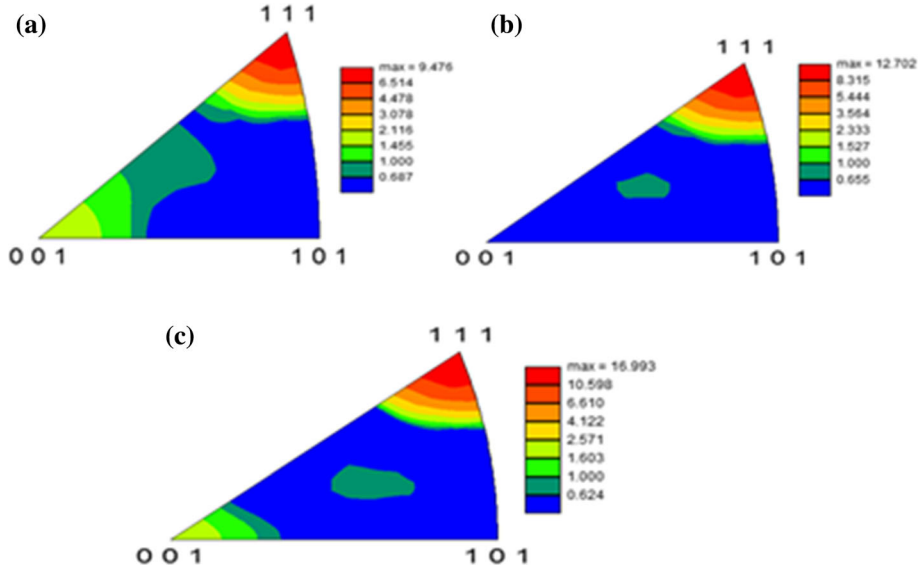

Fig. 7 Inverse pole figures on (100) (the plane perpendicular to ED) of the composite extruded with different extrusion ratios (a) R-11@GNPs/Al; (b) R-17@GNPs/Al; (c) R-25@GNPs/Al

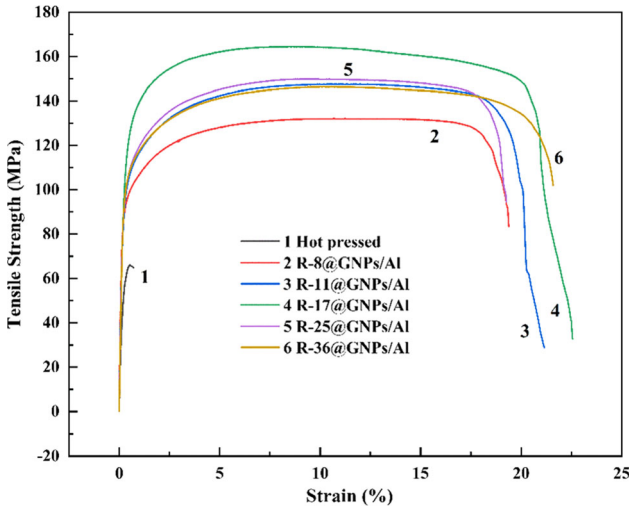

Fig. 8 Stress–strain curves of the composite hot-pressed or extruded with different extrusion ratios

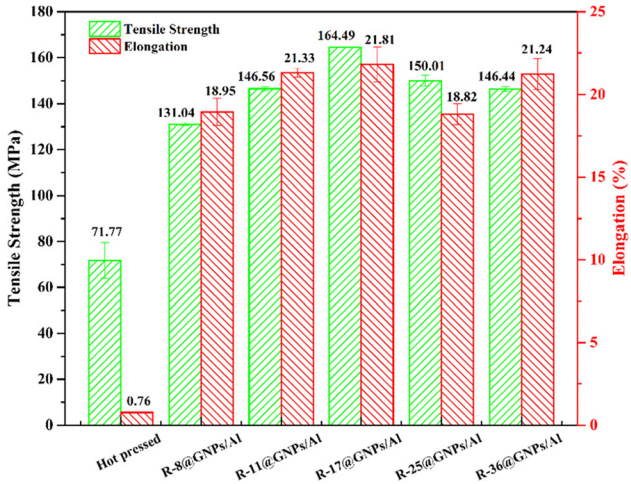

Fig. 9 Tensile strength and elongation of the composite hot-pressed or extruded with different extrusion ratios

of 40.28HV; the hardness of the R-17@GNPs/Al composite is 45.5HV; the R-25@GNPs/Al composite shows the best hardness, with a value of 45.69HV, which is slightly higher than that of R-17@GNPs/Al. With increasing extrusion ratio, the three-dimensional compressive stress of the composite during the extrusion process increases, the work hardening effect is obvious (Fig. 6e, f), and the hardness of the composite is significantly improved. However, when the extrusion ratio reaches 36:1, the integrity of the GNPs is destroyed (referring to the analysis for Fig. 4), reducing the hardness of the composite.

3.3 Morphology of the Tensile Fracture

Figure 13 shows the SEM morphology for the tensile fracture section of the composite. It can be seen from Fig. 13(a) and (b) that the GNP and the matrix do not bond well and intergranular fractures play the dominant role. The layers between the GNP or the interface between the GNP and the matrix give rise to the crack initiations. The tensile fracture of the R-8@GNPs/Al composite presents a partial brittle fracture with fewer dimples and an uneven distribution. It can be observed from Fig. 13(d) and (f) that when the extrusion ratio is relatively small, GNPs with more layers are observed (inside

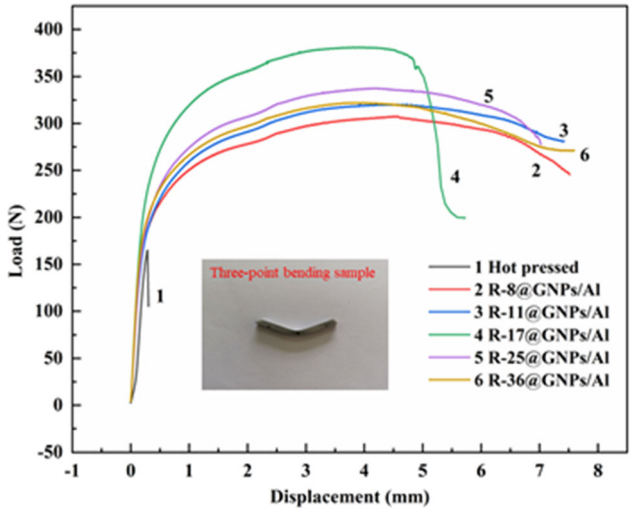

Fig. 10 The three-point bending load–displacement curves of the composite hot-pressed or extruded with different extrusion ratios

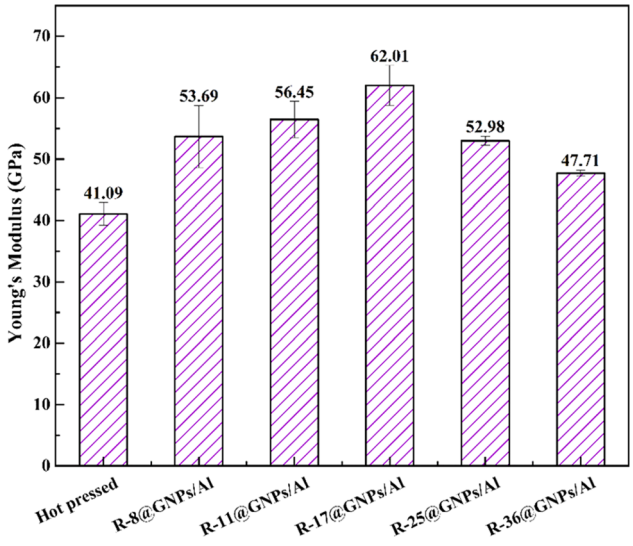

Fig. 11 Young's modulus of the composite hot-pressed or extruded with different extrusion ratios

the large dimples or on the relatively thick tearing edges). Therefore, the interface between GNP layers or the interface between GNPs and the matrix still initiates the cracks. With an increase in the extrusion ratio, especially with the extrusion ratio of 17:1, the grain size decreases (Fig. 5c, d) because of dynamic recrystallization, so the dimples become small and deep, whose number increases greatly, improving the tensile strength of the composite (Ref 38). Furthermore, it can be observed in Fig. 13(h) that the tearing edge of the dimples is thin and bright, which indicates that the layer number of the GNPs is small (Fig. 4f), and the interface bond is strong between the GNPs and the aluminum matrix. This is further supported by the element distribution for the tensile fracture section of the composite extruded with an extrusion ratio of 17:1 shown in Fig. 14, in which the C element is mainly distributed on the segregated GNPs in the large dimples and on the tearing edges. The load on the aluminum matrix is effectively transferred to the GNPs so that the composite can

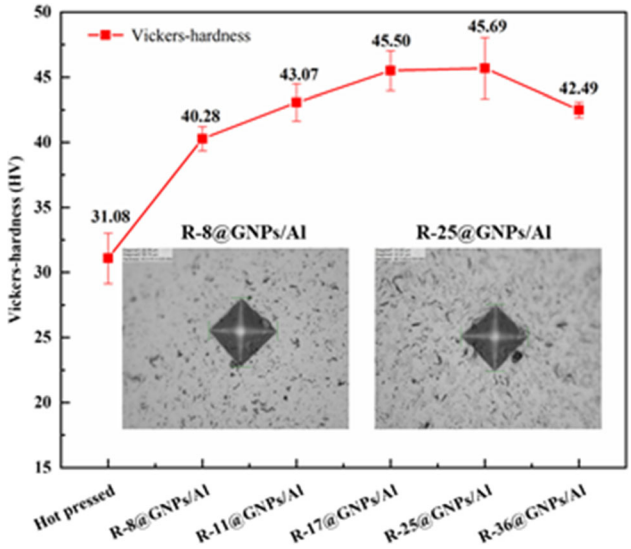

Fig. 12 Vickers hardness of the composite extruded with different extrusion ratios

show enhanced properties. R-25@GNPs/Al shows the best GNP integrity and the least layers, but its grain size is larger (as shown in Fig. 5), resulting in relatively low comprehensive properties. As the extrusion ratio continues to increase to 36:1, the extreme deformation will lead to a more local temperature increase and growth of the matrix grains. Moreover, the size of the GNP decreases, as further proven in Fig. 13(l), which is consistent with the results from Raman spectroscopy (Fig. 4f). GNP with a smaller diameter is not conducive to load transfer, resulting in a decline in the enhancement efficiency of GNP.

4. Conclusions

In this paper, a 0.5 wt.% GNP/Al composite was hot extruded with different extrusion ratios. The effect of the extrusion ratio on the composite was explored. The main conclusions are as follows:

(1) The extrusion ratio is an important parameter that influences the strength efficiency for hot extrusions of the microstructure and mechanical performance of the 0.5 wt.% GNP/Al composite.
(2) For the five different extrusion ratios (8:1, 11:1, 17:1, 25:1 and 36:1), the tensile properties, bending strength, bending stiffness and Young's modulus reach the best values at an extrusion ratio of 17:1, while the hardness and the bending toughness are the highest with an extrusion ratio of 25:1, mainly because of the better work hardening and high structural integrity and the least layers of the GNPs compared to the composite extruded with a ratio of 17:1.
(3) The microstructures and mechanical properties of the extruded composite mainly depend on the combined effects of work hardening or dynamic recrystallization and dynamic recovery of the grains, the state of the GNPs, and the interface between the GNPs and the matrix, all of which are influenced by the extrusion ratio.

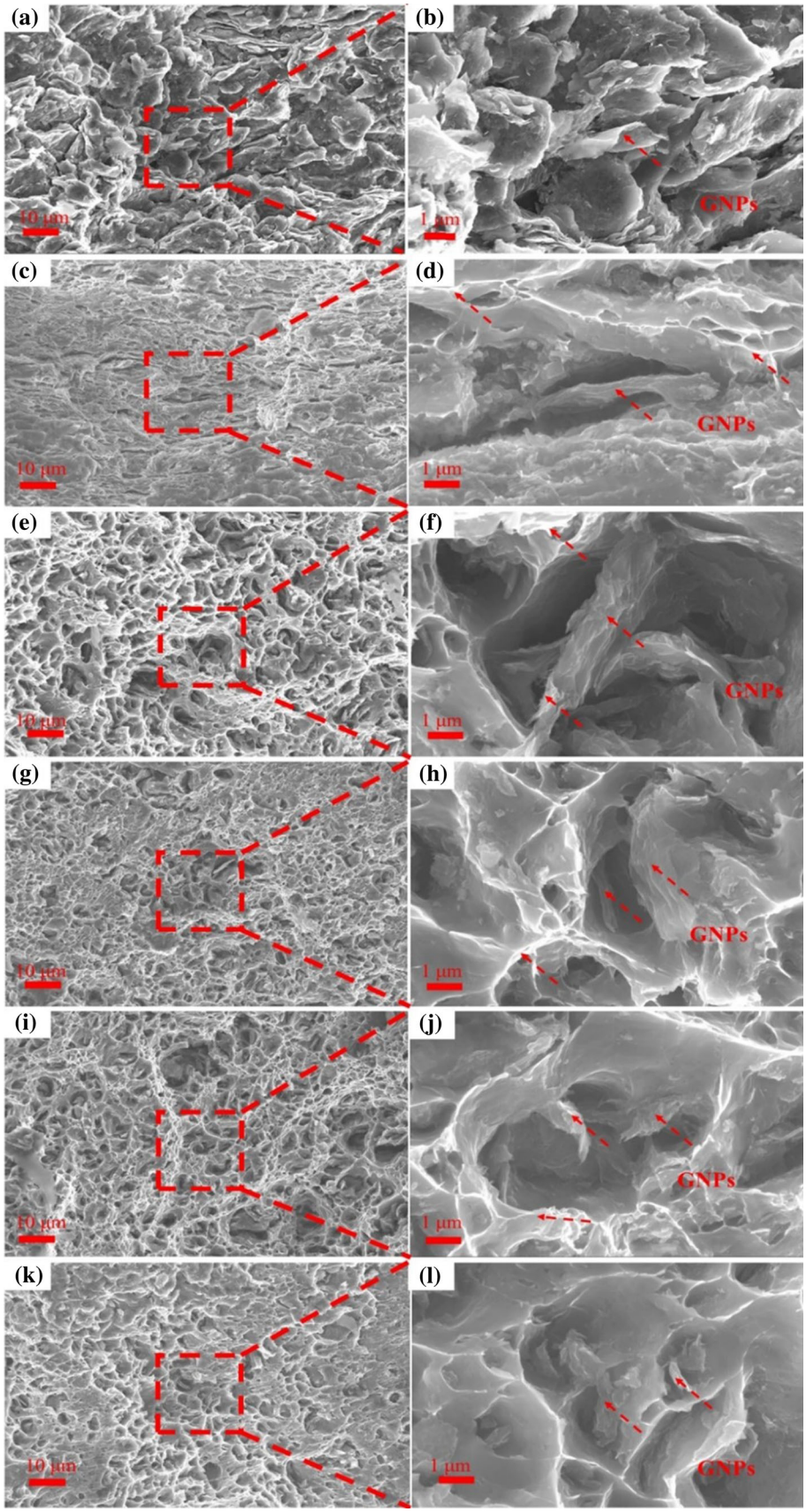

Fig. 13 SEM morphology on tensile fracture section of the composite hot-pressed and extruded with different extrusion ratios: (a, b) hot-pressed; (c, d) R-8@GNPs/Al; (e, f) R-11@GNPs/Al; (g, h) R-17@GNPs/Al; (i, j) R-25@GNPs/Al; (k, l) R-36@GNPs/Al

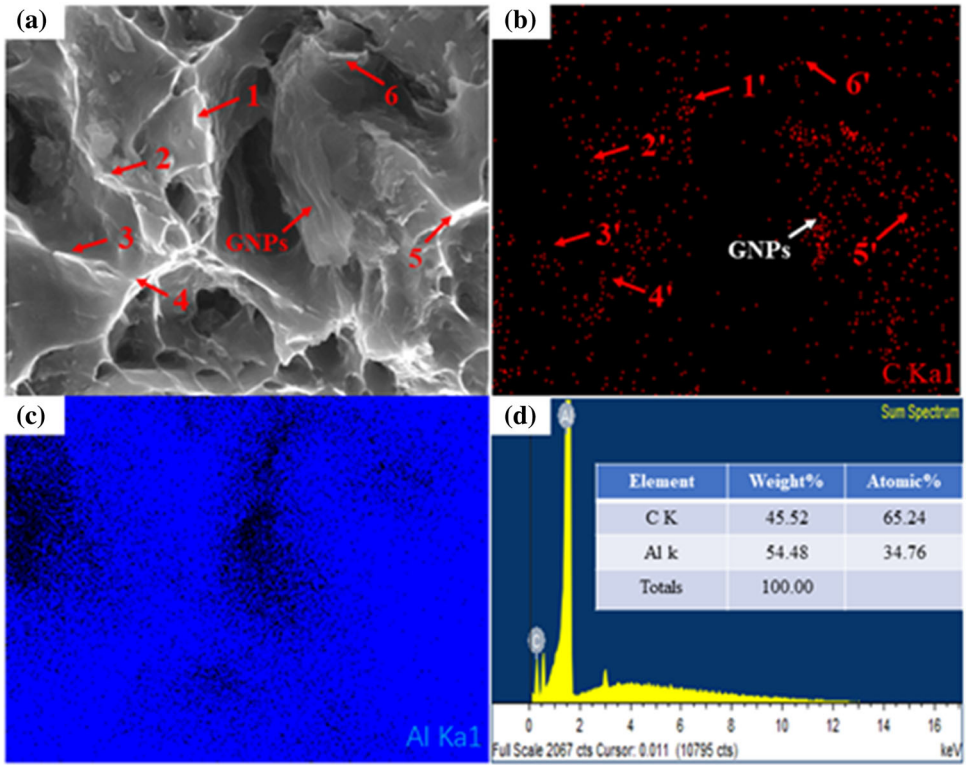

Fig. 14 Elements distribution on the tensile fracture section of the composite extruded with extrusion ratio of 17:1

5. Conflict of interest

The authors declare no conflict of interest.

Acknowledgments

This work was financially supported by National Natural Science Foundation of China (Nos. 51705295, 51778351), Key project of the Shandong Provincial Natural Science Foundation, China (ZR2020KE013) and Shandong University of Science and Technology Research Fund of China (No. 2018TDJH101). University Qing Chuang science and technology plan of Shandong (No. 2019KJB015)

References

1. F. Mokdad, D.L. Chen, Z.Y. Liu, B.L. Xiao, D.R. Ni and Z.Y. Ma, Deformation and Strengthening Mechanisms of a Carbon Nanotube Reinforced Aluminum Composite, *Carbon*, 2016, **104**, p 64-77
2. E.I. Salama, A. Abbas and A.K. Esawi, Preparation and Properties of Dual-Matrix Carbon Nanotube-Reinforced Aluminum Composites, *Compos. A*, 2017, **99**, p 84-93
3. N.S. Pourmand and H. Asgharzadeh, Aluminum Matrix Composites Reinforced with Graphene: A Review on Production Microstructure and Properties, *Crit. Rev. Solid State Mater. Sci.*, 2019, **45**(4), p 289–337
4. B.S. Guo, M. Song, J.H. Yi, S. Ni, T. Shen and Y. Du, Improving the Mechanical Properties of Carbon Nanotubes Reinforced Pure Aluminum Matrix Composites by Achieving Non-Equilibrium Interface, *Mater. Des.*, 2017, **120**, p 56-65
5. Z. Zheng, X.X. Zhang, J.C. Li and L. Geng, High-Content Graphene Nanoplatelet Reinforced Aluminum Composites Produced by Ball Milling and Hot Extrusion, *Sci. China*, 2020, **63**(08), p 1426-1435
6. T.L. Han, F.C. Wang, J.J. Li, N.Q. Zhao and C.N. He, Simultaneously Enhanced Strength and Ductility of Al matrix composites through the Introduction of Intragranular Nano-Sized Graphene Nanoplates, *Compos. Part B*, 2021, **212**, p 108700
7. Y.M. Xie, X.C. Meng, Y.X. Huang, J.C. Li and J. Cao, Deformation-Driven Metallurgy of Graphene Nanoplatelets Reinforced Aluminum Composite for the Balance between Strength and Ductility, *Compos. Part B.*, 2019, **177**, p 107413
8. S.M. Lou, Y.Q. Liu, C.D. Qu, G.X. Guo, L.W. Ran, P.P. Zhang and C.J. Su, Influence of a Hot Extrusion with Rectangular Section on Mechanical Properties and Microstructure of 0.5 wt% Graphene Nanoplate-Reinforced Aluminum Composites, *Adv. Eng. Mater.*, 2021, **23**(4), p 2001127
9. B.Y. Ju, W.S. Yang, P.Z. Shao, M. Hussain, Q. Zhang, Z.Y. Xiu, X.W. Hou, J. Qiao and G.H. Wu, Effect of Interfacial Microstructure on the Mechanical Properties of GNPs/Al Composites, *Carbon*, 2020, **162**, p 346-355.
10. Y.Y. Jiang, R. Xu, Z.Q. Tan, G. Ji, G.L. Fan, Z. Li, D.B. Xiong, Q. Guo, Z.Q. Li and D. Zhang, Interface-Induced Strain Hardening of Graphene Nanosheet/Aluminum Composites, *Carbon.*, 2019, **146**, p 17-27.
11. W.S. Yang, Q.Q. Zhao, L. Xin, J. Qiao, J.Y. Zou, P.Z. Shao, Z.H. Yu, Q. Zhang and G.H. Wu, Microstructure and Mechanical Properties of Graphene Nanoplates Reinforced Pure Al Matrix Composites Prepared by Pressure Infiltration Method, *J. Alloys Compd*, 2018, **732**, p 748-758.
12. N.S. Anas, M. Ramakrishna and R. Vijay, Microstructural Characteristics and Mechanical Properties of CNT/Ni Coated CNT–Dispersed Al Alloys Produced by High Energy Ball Milling and Hot Extrusion, *Met. Mater. Int.*, 2020, **26**(2), p 272-283
13. H.P. Zhang, C. Xu, W.L. Xiao, K. Ameyama and C.L. Ma, Enhanced Mechanical Properties of Al5083 Alloy with Graphene Nanoplates Prepared by Ball Milling and Hot Extrusion Mater, *Sci. Eng.*, 2016, **658**, p 8-15
14. A. Saboori, R. Casati, A. Zanatta, M. Pavese, C. Badini and M. Vedani, Effect of Graphene Nanoplatelets on Microstructure and Mechanical Properties of AlSi10Mg Nanocomposites Produced by Hot Extrusion, *Powder Metall. Met. Ceram.*, 2018, **56**(11–12), p 647-655

15. Z.F. Wei, Y.S. Lei, H. Yan, X.H. Xu and J.J. He, Microstructure and Mechanical Properties of A356 Alloy with Yttrium Addition Processed by Hot Extrusion, *J. Rare Earths*, 2019, **37**(6), p 659-667
16. F. Mokdad, D.L. Chen, Z.Y. Liu, D.R. Ni, B.L. Xiao and Z.Y. Ma, Hot Deformation and Activation Energy of a CNT-Reinforced Aluminum Matrix Nanocomposite, *Mater. Sci. Eng.*, 2017, **695**, p 322-331
17. D. Jeyasimman, K. Sivaprasad, S. Sivasankaran and R. Narayanasamy, Fabrication and Consolidation Behavior of Al 6061 Nanocomposite Powders Reinforced by Multi-Walled Carbon Nanotubes, *Powder Technol.*, 2014, **258**, p 189-197
18. S. Wang, T.T. Zheng, M. Xie, A. Li and P. Hou, Densification Behavior of Ag-Graphene Composites Prepared by Low-pressure Compressing and Vacuum Sintering, *Rare Met. Mater. Eng.*, 2019, **48**(11), p 3494
19. L.Y. Sheng, X.R. Zhang, H. Zhao and B.N. Du, Influence of Multi-Pass Hot Extrusion on Microstructure and Mechanical Properties of the Mg–4Zn–1.2Y–0.8Nd Alloy, *Crystals*, 2021, **11**(4), p 425
20. P.Z. Shao, W.S. Yang, Q. Zhang, Q.Y. Meng, X. Tan, Z.Y. Xiu, J. Qiao, Z.H. Yu and G.H. Wu, Microstructure and Tensile Properties of 5083 Al Matrix Composites Reinforced with Graphene Oxide and Graphene Nanoplates Prepared by Pressure Infiltration Method, *J. Composites, Part A.*, 2018, **109**, p 151-162
21. C.H. Li, R.S. Qiu, B.F. Luan and Z.Q. Li, Effect of Carbon Nanotubes and High Temperature Extrusion on the Microstructure Evolution of Al-Cu Alloy, *Mater. Sci. Eng A*, 2017, **704**, p 38-44
22. Z.Y. Xu, C.J. Li, K.R. Li, J.H. Yi, J.J. Tang, Q.X. Zhang, X.Q. Liu, R. Bao and X. Li, J Carbon Nanotube-Reinforced Aluminum Matrix Composites Enhanced by Grain Refinement and In Situ Precipitation, *Mater. Sci.*, 2019, **54**(11), p 8655-8664
23. X.J. Wang, X.M. Wang, X.S. Hu and K. Wu, Effects of Hot Extrusion on Microstructure and mechanical Properties of Mg Matrix Composite Reinforced with Deformable TC_4 Particles, *J. Magnesium Alloys.*, 2020, **8**, p 421-430
24. Q. Yang, D.L. Cheng, J. Liu, L. Wang, Z. Chen, M.L. Wang, S.Y. Zhong, Y. Wu, G. Ji and H.W. Wang, Microstructure Evolution of the TiB_2/Al Composites Metallurgy during Hot Extrusion, *Mater. Charact.*, 2019, **155**, p 109834
25. A. Güzel, A. Jäger, F. Parvizian, H.G. Lambers, A.E. Tekkaya, B. Svendsen and H.J. Maier, A New Method for Determining Dynamic Grain Structure Evolution during Hot Aluminum Extrusion, *J. Mater. Process. Technol.*, 2012, **212**(1), p 323–320
26. Z.C. Sun, L.S. Zheng and H. Yang, Softening Mechanism and Microstructure Evolution of as-Extruded 7075 Aluminum Alloy during Hot Deformation, *Mater. Charact.*, 2014, **90**, p 71-80
27. A. Ditta, L.J. Wei, Y.J. Xu and S.J. Wu, Effect of Hot Extrusion and Optimal Solution Treatment on Microstructure and Properties of Spray-Formed Al-11.3Zn-2.65Mg-1Cu Alloy, *J. Alloys Compd.*, 2019, **797**, p 558-565
28. X. Lei, R.C. Wang, C.Q. Peng, Y. Feng and Y.H. Sun, Effect of Hot Extrusion on the Microstructure, Mechanical Properties, and Corrosion Behavior of Mg–11Li–3Al–2Zn–1.5Nd–0.2Zr Alloy, *Trans. Indian Inst. Met.*, 2019, **72**(10), p 2893–2899
29. P.Z. Shao, G.Q. Chen, W.S. Yang, Q. Zhang, B.Y. Ju, Z.J. Wang, X. Tan, Y.Y. Pei, S.J. Zhong, M. Hussain and G.H. Wu, Effect of Hot Extrusion Temperature on Graphene Nanoplatelets Reinforced Al6061 Composite Fabricated by Pressure Infiltration Method, *Carbon*, 2020, **162**, p 455-464
30. Z.J. Yu, C. Xu, J. Meng, K. Liu, J.L. Fu and S. Kamado, Effects of Extrusion Ratio and Temperature on the Mechanical Properties and Microstructure of as-Extruded Mg-Gd-Y-(Nd/Zn)-Zr Alloys, *Mater. Sci. Eng. A.*, 2019, **762**, p 138080
31. M.M. El-S, M.M.Z. Seleman and S.A. Ahmed, Microstructure and Mechanical Properties of Hot Extruded 6016 Aluminum Alloy/Graphite Composites, *J. Mater. Sci. Technol.*, 2018, **34**(09), p 1580–1591
32. S.M. Lou, C.D. Qu, G.X. Guo, L.W. Ran, Y.Q. Liu, P.P. Zhang, S. Chun Jian and Q.B. Wang, Effect of Fabrication Parameters on the Performance of 0.5 wt.% Graphene Nanoplates-Reinforced Aluminum Composites, *Materials*, 2020, **13**(16), p 3483. https://doi.org/10.3390/ma13163483
33. R.V. Kumar, R. Harichandran, U. Vignesha, M. Thangavel and S.B. Chandrasekhar, Influence of Hot Extrusion on Strain Hardening Behaviour of Graphene Platelets Dispersed Aluminium Composites, *J. Alloys Compd.*, 2021, **855**, p 157448
34. W.M. Jiang, J.W. Zhu, G.Y. Li, F. Guan, Y. Yu and Z.T. Fan, Enhanced Mechanical Properties of 6082 Aluminum Alloy Via SiC Addition Combined with Squeeze Casting, *J. Mater. Sci. Technol.*, 2021, **88**, p 119–131
35. J.W. Zhu, W.M. Jiang, G.Y. Li, F. Guan, Y. Yu and Z.T. Fan, Microstructure and Mechanical Properties of SiCnp/Al6082 Aluminum Matrix Composites Prepared by Squeeze Casting Combined with Stir Casting, *J. Mater. Process. Technol.*, 2020, **283**, p 116699
36. B.N. Du, Z.Y. Hu, L.Y. Sheng, D.K. Xu, Y.X. Qiao, B.J. Wang, J. Wang, Y.F. Zheng and T.F. Xi, Microstructural Characteristics and Mechanical Properties of the Hot Extruded Mg-Zn-Y-Nd Alloys, *J. Mater. Sci. Technol.*, 2021, **01**, p 44–55
37. D.H. Nam, S.I. Cha, B.K. Lima, H.M. Park, D.S. Han and S.H. Hong, Synergistic Strengthening by Load Transfer Mechanism and Grain Refinement of CNT/Al–Cu Composites, *Carbon*, 2012, **50**, p 2417-2423
38. W.M. Jiang, Z.T. Fan, Y.C. Dai and C. Li, Effects of Rare Earth elements Addition on Microstructures, Tensile Properties and Fractography of A357 Alloy, *J. Mater. Sci. Eng. A*, 2014, **597**(3), p 237-244